
REAL IMAGE SUPER RESOLUTION VIA HETEROGENEOUS MODEL ENSEMBLE USING GP-NAS

A PREPRINT

Zhihong Pan, Baopu Li
Baidu Research (USA)

Teng Xi, Yanwen Fan, Gang Zhang, Jingtuo Liu, Junyu Han, Errui Ding
Department of Computer Vision Technology (VIS), Baidu Inc.

ABSTRACT

With advancement in deep neural network (DNN), recent state-of-the-art (SOTA) image super-resolution (SR) methods have achieved impressive performance using deep residual network with dense skip connections. While these models perform well on benchmark dataset where low-resolution (LR) images are constructed from high-resolution (HR) references with known blur kernel, real image SR is more challenging when both images in the LR-HR pair are collected from real cameras. Based on existing dense residual networks, a Gaussian process based neural architecture search (GP-NAS) scheme is utilized to find candidate network architectures using a large search space by varying the number of dense residual blocks, the block size and the number of features. A suite of heterogeneous models with diverse network structure and hyperparameter are selected for model-ensemble to achieve outstanding performance in real image SR. The proposed method won the first place in all three tracks of the AIM 2020 Real Image Super-Resolution Challenge.

1 Introduction

Image super-resolution (SR) refers the process to recover high-resolution (HR) images from low-resolution (LR) inputs. It is an important image processing technique to enhance image quality which subsequently helps to improve higher-level computer vision tasks [3] [8]. Over the years, many classical SR methods have been proposed to successfully use various levels of features like statistics [24], edges [26] [27] and patches [28] [31] to restore HR images from LR inputs. While there are also methods developed for SR using multiple frames [10], the scope of introduction here is limited to single image super-resolution (SISR).

More recently, the powerful deep learning techniques have led to developments of many deep learning based SR models [4] [12] [14] [17] [34] [33]. These deep learning models commonly rely on a large set of synthetic training image pairs, where the LR input is downsampled from the HR reference image using bicubic interpolation with antialiasing filters. Common image quality metrics used to assess performance of these SR models include peak signal-to-noise ratio (PSNR) and the structural similarity index (SSIM) [35], both emphasizing image restoration fidelity by comparing to the HR reference. This may lead to SR results of high PSNR values but lack of HR details perceptually. Lately, a new metric LPIPS [32] is proposed to apply image features extracted from pretrained Alexnet [13] to compare two images. The smaller LPIPS is, the closer the generated SR image is to the HR reference perceptually. With advancements in Generative Adversarial Nets (GAN) [5], SR models trained using GAN [29] [21] [9] have achieved the best performance of image perceptual quality as compared to LPIPS.

In the past few years, neural architecture search (NAS) that aims to find the optimal network structure has received a lot of attention [19] [36] [37] [18]. It effectively boosts the SOTA in many typical computer vision problems such as image classification [20], object detection [16], segmentation [1] and so on. Most recently, some researches also begin to apply NAS for image SR problems [2] [25] [7] with impressive results using efficient SR models.

In general, the SR problem is ill-posed as there are multiple HR images corresponding to a single LR image even when the LR image is constructed from the HR reference using bicubic interpolation without added noise. This ambiguity increases when the blur kernel and noise statistics of the LR are not known, and is even more prominent in real image SR problems where the LR image is not constructed from the HR reference. With the increased uncertainty, it is common to see different deep learning SR models lead to different versions of the restored HR images for a single LR image, especially when the network architectures are quite different. To achieve the best performance of the real image SR problem set forth by the AIM 2020 challenge, a new fusion scheme is proposed in this study to generate the final

SR output using multi-level ensemble from a suite of heterogeneous deep learning models that are obtained by applying NAS approach. The main contributions of the proposed method include:

- A Gaussian Process based NAS (GP-NAS) is first utilized for super-resolution with specially designed search space, which can efficiently search and obtain the key architecture related parameters and can yield multiple candidate models.
- A multi-level ensemble scheme is proposed in testing, including self-ensemble for patches, as well as patch-ensemble and model-ensemble for full-size images.
- The proposed method was applied for the AIM 2020 Real Image Super-Resolution Challenge and won the first place in all three tracks (upsampling factors of $\times 2$, $\times 3$ and $\times 4$) with a comfortable margin in both PSNR and SSIM.

2 Related Works

Deep Learning for Single Image Super-Resolution. As the first successful application, Dong *et al.* [4] proposed a deep CNN model for end-to-end LR to HR mapping and showed that the training of the neural network is equivalent to global optimization of traditional sparse-coding-based SR methods. Kim *et al.*[12] designed a deeply recursive neural network to raise SR performance without increasing parameters for additional convolutions. Ledig *et al.*[14] were the first to use GAN for SR, introducing a perceptual loss function to generate photo-realistic SR images from LR inputs. Inspired by other SR models using deep residual networks [11] [12], Lim *et al.*[17] simplified the network structure by removing BN layers and optimized the training process to achieve the best restoration fidelity at that time. Zhang *et al.* first applied dense skip-connections [34] and later channel attention module [33] in deep residual network for further advancing of SOTA. Most recently, Guo *et al.*[6] proposed a dual-regression method by adding a second downsampling model and corresponding loss to make sure the restored SR image can best match the LR input after downsampled by the co-trained secondary model.

NAS for Single Image Super-Resolution. As the first attempt to apply NAS for SR, Chu *et al.*[2] made use of an elastic search method on both micro and macro level with a hybrid controller that profits from evolutionary computation and reinforcement learning (RL), achieving comparable performance of PSNR with light model. Based on different types of residual blocks and evolutionary algorithm, Song *et al.*[25] proposed a search method for better and more efficient network for image SR. Guo *et al.*[7] put forward a novel hierarchical NAS approach that considers both the cell-level and network-level design based on a RL controller. While all the three works are promising at searching for efficient SR models where resources like model size or FLOPS are limited, they are not able to achieve the high PSNR or SSIM values comparing to other SOTA methods using manually designed residual networks with dense skip connections. Aiming at AIM 2020 challenge that does not take model efficiency in consideration, we mainly concentrate on the macro level structure design for a better network structure that can achieve the best SR performance in terms of PSNR and SSIM. Moreover, instead of using RL or evolutionary based search method that tend to be very time consuming, we apply GP-NAS approach to search the key network structure parameters such as the number of dense residual block, the block size and the number of features.

3 Problem Formulation

Learning based image SR methods often rely on a large number of image pairs, including low-res image \mathbf{I}_{LR} and reference high-res \mathbf{I}_{HR} . For real image SR, as shown in Eq. 1, \mathbf{I}_{LR} could be modeled from \mathbf{I}_{HR} using three steps: convolution with a kernel \mathbf{k} , downsampling $D_s(\cdot)$ and addition of noise \mathbf{n} .

$$\mathbf{I}_{LR} = D_s(\mathbf{I}_{HR} * \mathbf{k}) + \mathbf{n} \quad (1)$$

The goal of image SR is to reverse this process, finding the matching \mathbf{I}_{HR} from a known \mathbf{I}_{LR} . This problem is challenging as there are many versions of \mathbf{I}_{HR} that could generate the same \mathbf{I}_{LR} following the process in Eq. 1, even when the kernel \mathbf{k} is known and there is no noise \mathbf{n} . Learning based SR model $f(\cdot)$ use a total of n image pairs to minimize the average error as in Eq. 2. It is common that only \mathbf{I}_{HR}^i is a real image and the corresponding \mathbf{I}_{LR}^i is constructed from \mathbf{I}_{HR}^i following the process described in Eq. 1.

$$\arg \min_f \sum \|f(\mathbf{I}_{LR}^i) - \mathbf{I}_{HR}^i\|, i \in \{1, 2, \dots, n\} \quad (2)$$

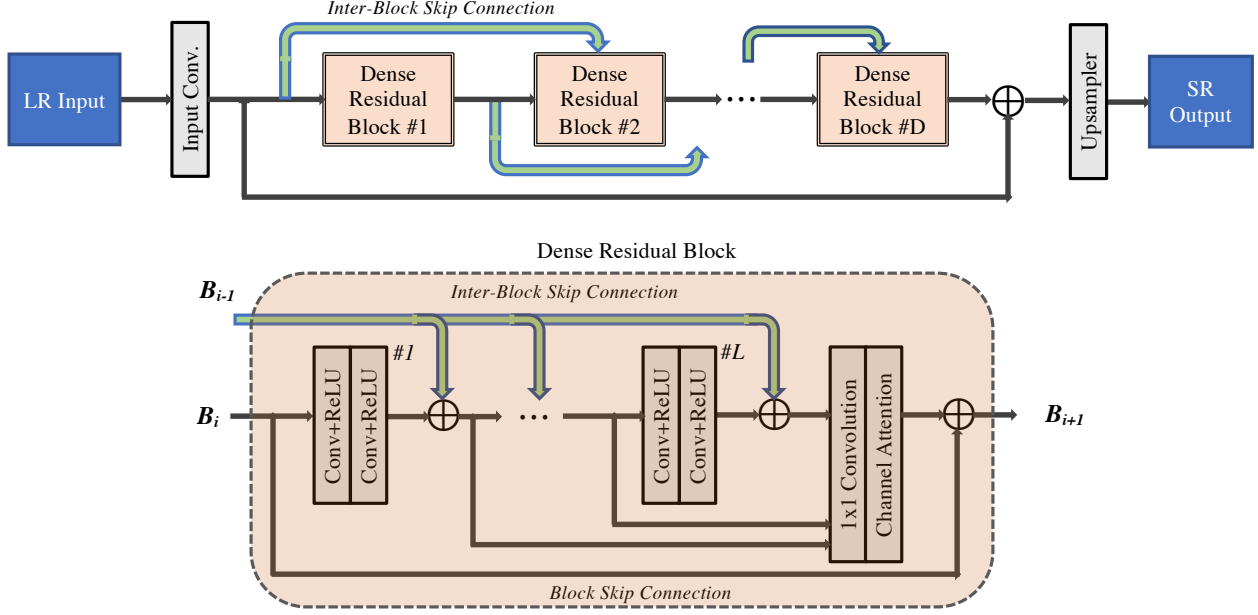


Figure 1: The deep dense residual network architecture for image super resolution.

In the case that both \mathbf{I}_{HR} and \mathbf{I}_{LR} are real images collected separately, the relationship between the image pair is much more complicated. To get a digital image \mathbf{I} from an object \mathbf{O} , there are three transformations included in general as shown in Eq. 3. The optical transformation $\mathbb{O}(\cdot)$ refers to the process of photons reflected from the object passing through the lens of the camera. Optical characteristics of the lens like modulation transfer function (MTF) and lens settings like aperture are key variables here. The second transformation $\mathbb{D}(\cdot)$ refers to the analog to digital converter (ADC) that turns photons to digital numbers, where the noise is introduced. The last one $\mathbb{I}(\cdot)$ refers to the image signal processor (ISP) which transforms noisy raw images to end result of sRGB images. This step is the most complicated of three, including multiple processes like denoising and color balancing at both global and local levels.

$$\mathbf{I} = \mathbb{I}(\mathbb{D}(\mathbb{O}(\mathbf{O}))) \quad (3)$$

As each of the three transformations could be different for HR and LR images, the relationship between \mathbf{I}_{LR} and \mathbf{I}_{HR} can be illustrated as in Equations 4-6 where they are linked indirectly by the downsampling of \mathbf{O}_{HR} to \mathbf{O}_{LR} using $D_s(\cdot)$. With all these added variations, the real image SR becomes more challenging. For example, \mathbf{I}_{HR} is more clear in general compared to \mathbf{I}_{LR} . But for background objects at a further distance, they could be more blurry in \mathbf{I}_{HR} if its lens has a smaller f-number which lead to smaller depth-of-field. The motivation to use heterogeneous model ensemble is based on the observation that different model could lead to optimization results biased towards different variation factors even when using the same set of training image pairs.

$$\mathbf{I}_{LR} = \mathbb{I}_{LR}(\mathbb{D}_{LR}(\mathbb{O}_{LR}(\mathbf{O}_{LR}))) \quad (4)$$

$$\mathbf{I}_{HR} = \mathbb{I}_{HR}(\mathbb{D}_{HR}(\mathbb{O}_{HR}(\mathbf{O}_{HR}))) \quad (5)$$

$$\mathbf{O}_{LR} = D_s(\mathbf{O}_{HR}) \quad (6)$$

4 Proposed Real Image SR Method

The proposed real image SR method using dense residual network, GP-NAS and heterogeneous model ensemble is explained in this section. First, the primary dense residual network and the search space of different hyperparameters are introduced. Then, method to find heterogeneous models using GP-NAS is explained, followed by the multi-level ensemble that is used to generate full-size SR images for the AIM 2020 challenge.

4.1 Dense Residual Network (DRN)

The backbone model of the proposed method is a deep dense residual network originally developed for raw image demosaicking and denoising. As depicted in Fig. 1, in addition to the shallow feature convolution at the front and the upsampler at the end, the proposed network consists of a total depth of D dense residual blocks (DRB). The input convolution layer converts the 3-channel LR input to a total of F -channel shallow features. For the middle DRB blocks, each one includes L stages of double layers of convolution and the outputs of all L stages are concatenated together before convoluted from $F \times L$ to F channels. An additional channel-attention layer is included at the end of each block, similar to RCAN [33]. There are two types of skip connections included in each block, the block skip connection (BSC) and inter-block skip connection (IBSC). The BSC is the shortcut between input and output of block B_i , while the IBSC includes two shortcuts from the input of block B_{i-1} to the two stages inside block B_i respectively. The various skip connections, especially IBSC, are included to combine features with a large range of receptive fields. The last block is an enhanced upsampler that transforms all F -channel LR features to the estimated 3-channel SR image. This dense residual network has three main hyperparameters: F is the number of feature channels, D is the number of DRB layers and L is the number of stages for each DRB. All these three hyperparameters will greatly affect the performance of SR. Previous efforts mainly use professional expertise or experience to choose them based on, which is laborious. To overcome this issue, we apply NAS to search for the optimal network structure, which will be elaborated in the subsequent subsection.

4.2 Gaussian Process based Neural Architecture Search

Since most NAS methods are still time consuming, we had proposed Gaussian Process based Neural Architecture Search (GP-NAS) [15] to accelerate the searching process. Figure 2 illustrates the framework of the GP-NAS. The GP-NAS formulates NAS from a Bayesian perspective. Specifically, given the hyper-parameters of GP-NAS, we are capable of predicting the performance of any architectures in the search space effectively. Then, the NAS process is converted to hyperparameters estimation. By mutual information maximization, we can efficiently sample networks. Accordingly, based on the performances of sampled networks, the posterior distribution of hyperparameters can be gradually and efficiently updated. Based on the estimated hyperparameters, the architecture with best performance can be obtained. More details about our proposed GP-NAS can be found in [15].

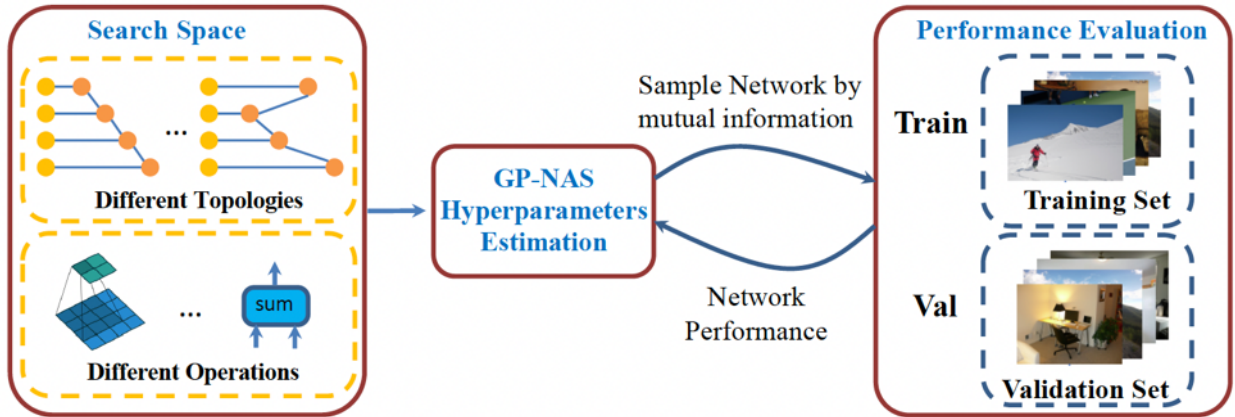


Figure 2: The framework of the GP-NAS.

4.3 Multi-Level Ensemble

Targeting for the AIM 2020 challenge, where the test images are much larger than the training patches, a multi-level ensemble scheme is designed to achieve optimal image restoration quality. First, for model-ensemble, the input LR image is processed by a suite of heterogeneous models separately and the output HR images are averaged to get the final output. Additionally, each full size LR input is cropped to patches, with each has an overlapping buffer with neighbouring patches. A patch-ensemble method is then used to blend all restored HR patches together, using different weights for each pixel which are correlated to the distance between the patch center and corresponding pixels. The most commonly used self-ensemble is also applied by flipping and/or transposing the input patch before restoration.

	Upscaling $\times 2$		Upscaling $\times 3$		Upscaling $\times 4$	
	PSNR	SSIM	PSNR	SSIM	PSNR	SSIM
DRN*	32.51 ¹	0.9209 ¹	31.07 ¹	0.8796 ¹	30.26 ³	0.8401 ³
RCAN*	32.31 ³	0.9188 ³	30.97 ³	0.8787 ³	30.31 ²	0.8403 ¹
RCAN	32.40 ²	0.9200 ²	31.01 ²	0.8792 ²	30.32 ¹	0.8402 ¹
DRN*+RCAN*	32.56 ²	0.9210 ²	31.21 ²	0.8811 ³	30.47 ³	0.8423 ¹
RCAN*+RCAN	32.49 ³	0.9204 ³	31.17 ³	0.8807 ³	30.48 ¹	0.8421 ³
DRN*+RCAN	32.62 ¹	0.9215 ¹	31.24 ¹	0.8814 ¹	30.48 ¹	0.8423 ¹
3-Model Ensemble	32.63	0.9218	31.28	0.8822	30.55	0.8435

Table 1: Quantitative results of single-model and model-ensemble methods. Best results are in bold and the ranks in each category are superscripted.

5 Experimental Results

The AIM 2020 challenge aims to find a generic model to super-resolve LR images captured in practical scenarios. To achieve this goal, paired LR and HR images were taken by various DSLR cameras. However, images used for training, validation and testing are captured in the same way with the same set of cameras, so the transformation processes described in Equations 4-6 are not changed among images of the same upscaling factor, meaning the learned transformation from training data is expected to achieve similar results on the validation and test images. For this new real image SR dataset, a total of 19,000 LR-HR pairs are available for model training for each of the $\times 2$, $\times 3$ and $\times 4$ upscaling factors. The LR image resolutions are 380×380 for $\times 3$, 272×272 for $\times 2$ and 194×194 for $\times 4$ respectively.

For our experiments of each upscaling factor, 600 of the 19,000 pairs are reserved for validation while the remaining ones are used for training. Note that any LR-HR pairs that are not perfectly aligned, those with normalized cross-correlation (NCC) less than 0.99, were excluded from both training and validation. For each epoch, a 120×120 patch is randomly cropped and augmented with flipping and transposing from each training image. A mixed loss of $L1$ and multi-scale structural similarity (MS-SSIM) is taken for training. For the experiment, the new model candidate search scheme using GP-NAS was implemented in PaddlePaddle [22] and the final-training of searched models were conducted using PyTorch [23]

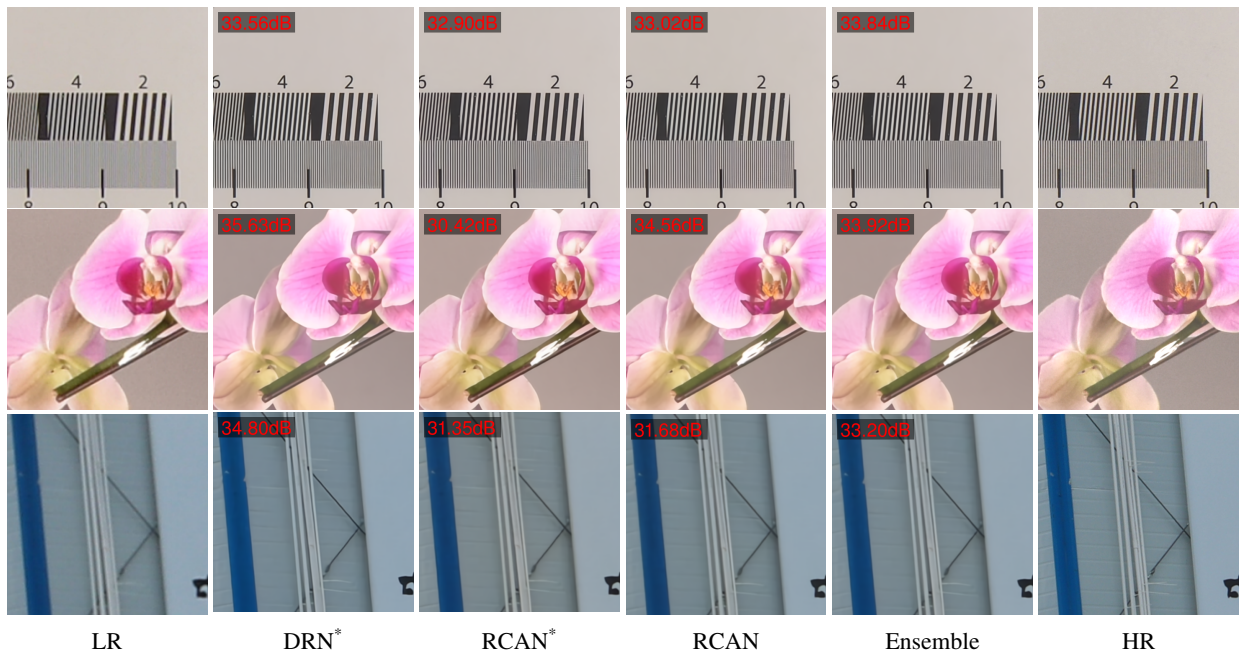


Figure 3: Visual and quantitative comparison of $\times 2$ SR results.

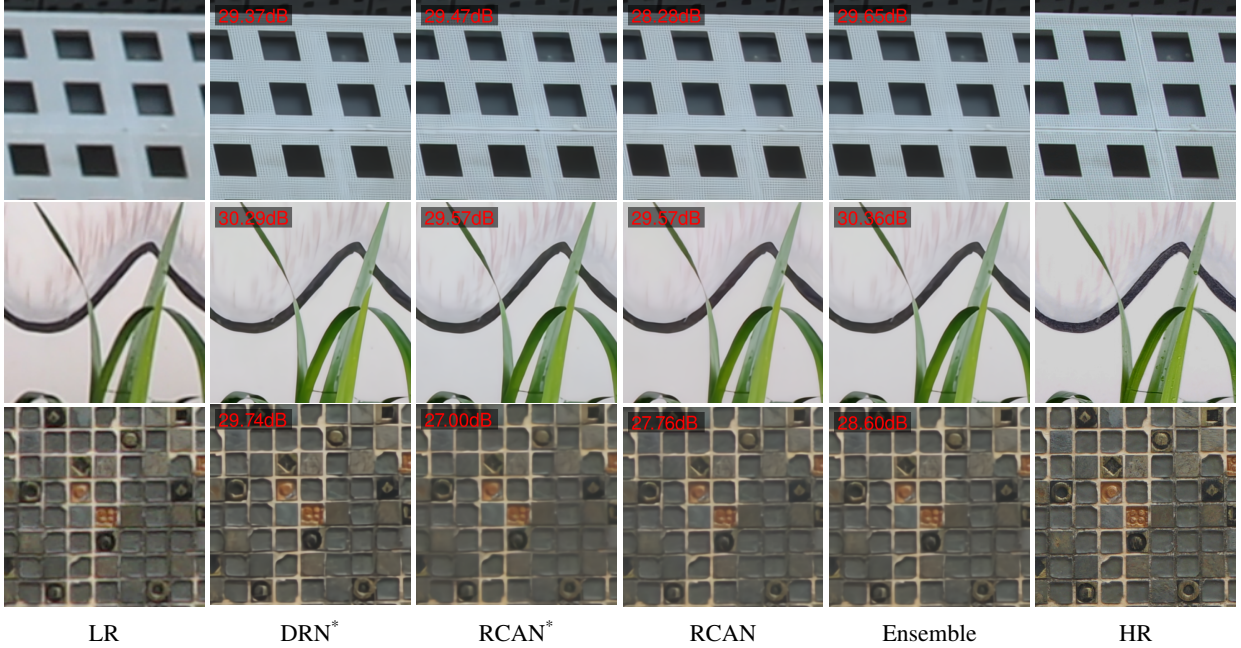


Figure 4: Visual and quantitative comparison of $\times 3$ SR results.

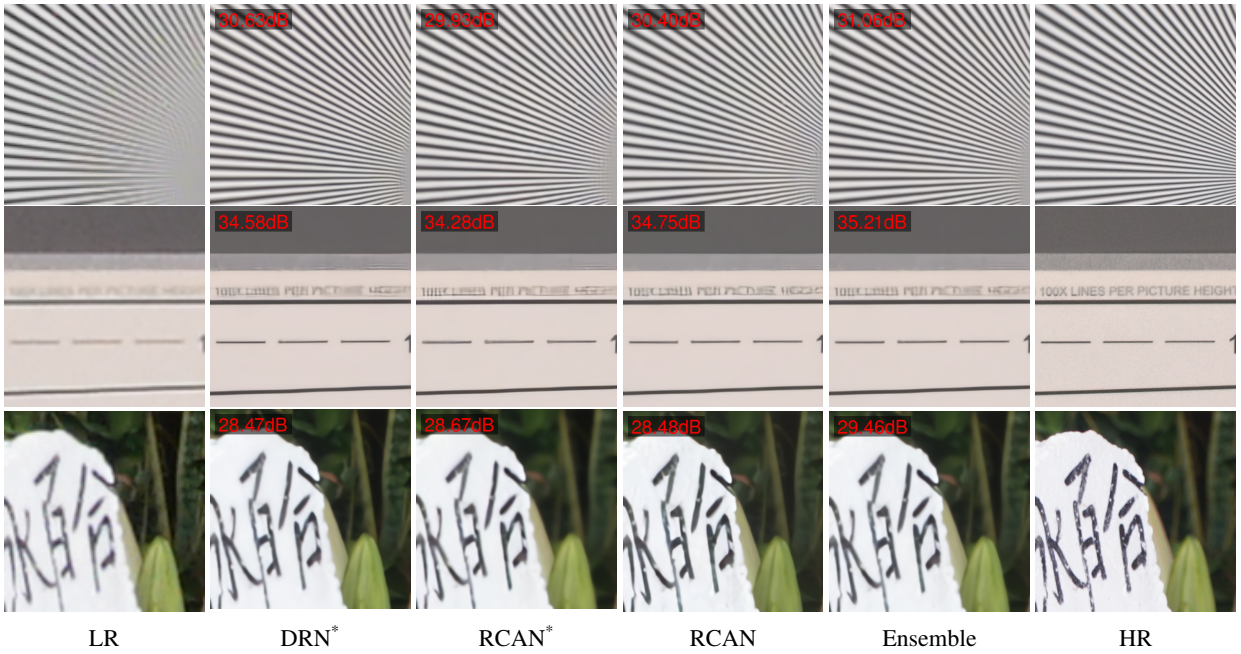


Figure 5: Visual and quantitative comparison of $\times 4$ SR results.

5.1 Ablation Study

Ablation studies were conducted to examine the effectiveness of the proposed heterogeneous model ensemble. Three models were trained for all three upscaling factors. DRN* is the selected DRN model using GP-NAS where $F = 128$, $D = 18$, $L = 3$. RCAN* is the GP-NAS selected variation of RCAN [33] with 128 features, 5 residual groups and 10 residual blocks in each group. And RCAN uses the original settings in [33] with 64 features, 10 residual groups and 20 residual blocks per group.

As shown in Table 1, the average performances of three individual models are very close. In general, DRN* is the best with RCAN as the close second. In comparison, results from model ensemble is always better than the individual models of the ensemble no matter it is a 2-model ensemble or 3-model one. Overall, the best results are always from the 3-model ensemble. One thing interesting to note is, out of three 2-model ensemble results, the one combining RCAN

and RCAN* is consistently worse than others. It could be explained that, for heterogeneous model ensemble, differences in network architecture is more beneficial than differences in hyperparameters of the same network architecture.

Some image examples are shown in Figures 3-5, where PSNR values of SR results are also annotated for quantitative comparison too. For small upscaling factor $\times 2$ as in Fig.3, there is no big difference among SR results visually. In the top example, individual SR models are all able to super-resolve the fine line features which are blurred in the LR input. By combining the models together, the ensemble result has higher PSNR than individual ones. But the other two examples show that the ensemble PSNR is lower than the best individual one. For the middle one, RCAN* seems to be the outlier comparing with the other two. Removing outlier before averaging would have increased the performance of ensemble. However, the outlier DRN* in the bottom example is the most accurate and removing it would lead to worse ensemble result.

Visual difference starts to stand out more in $\times 3$ examples as represented in Fig.4. For the first example on the top, all three individual models are able to super-resolve the small dot pattern which are blurred in LR input, but each is slightly different in details. By combining the models together, the ensemble result has higher PSNR than individual ones. The middle example also show ensemble result is higher than all individual ones and the visual difference are around the feather-like structures, showing different color and contrast. The bottom example shows DRN* has sharper image than the other two and its PSNR is higher than the ensemble as a result.

More interesting visual differences are observed in $\times 4$ examples as shown in Fig.5. For the first two examples, individual models resolve the blurred details differently, like the lines near right bottom right corner in the first and the small text in the second. While the ensemble result doesn't increase the image clarity, it has higher PSNR than all individual ones. The last one is worth noting as it demonstrates the difference in the optical transformation $\mathbb{O}(\cdot)$ for different cameras as explained in Section 3. The front object in HR image is clearer comparing to LR due to higher spatial resolution, but its background plant is more blurry than the LR counterpart, probably because the camera used for HR images has a smaller depth-of-field. The individual SR models handle this quite differently, with DRN* mimics the depth-of-field of the LR camera while the other two closer to the HR version. The ensemble method results in a significant increase in PSNR comparing to individual ones.

	Upscaling $\times 4$		Upscaling $\times 3$		Upscaling $\times 2$	
	PSNR	SSIM	PSNR	PSNR	PSNR	SSIM
Baidu (ours)	31.3960¹	0.8751¹	30.9496¹	0.8762¹	33.4460¹	0.9270¹
ALONG	31.2369 ²	0.8742 ³	30.3745 ⁵	0.8661 ⁶	33.0982 ⁸	0.9238 ⁶
CETC-CSKT	31.1226 ⁴	0.8744 ²	30.7651 ²	0.8714 ²	33.3140 ²	0.9245 ²
SR-IM	31.1735 ³	0.8728 ⁷	-	-	-	-
DeepBlueAI	30.9638 ⁶	0.8737 ⁴	30.3017 ⁷	0.8665 ⁴	33.1771 ⁷	0.9236 ⁷
JNSR	30.9988 ⁵	0.8722 ⁸	-	-	-	-
OPPO_CAMERA	30.8603 ⁸	0.8736 ⁵	30.5373 ⁴	0.8695 ³	33.3091 ³	0.9242 ⁴
Kailos	30.8659 ⁷	0.8734 ⁶	30.1303 ⁸	0.8664 ⁵	32.7084 ¹²	0.9196 ¹¹
SR_DL	30.6045 ⁹	0.8660 ¹²	-	-	-	-
Noah_TerminalVision	30.5870 ¹⁰	0.8662 ¹¹	30.5641 ³	0.8661 ⁷	33.2888 ⁴	0.9228 ⁸
Webbzhou	30.4174 ¹²	0.8673 ¹⁰	-	-	-	-
TeamInception	30.3465 ¹³	0.8681 ⁹	-	-	33.2322 ⁶	0.9240 ⁵
lyl	30.3191 ¹⁴	0.8655 ¹³	30.3654 ⁶	0.8642 ⁸	32.9368 ¹⁰	0.9210 ⁹
MCML-Yonsei	30.4201 ¹¹	0.8637 ¹⁵	-	-	32.9032 ¹¹	0.9186 ¹²
MoonCloud	30.2827 ¹⁵	0.8644 ¹⁴	-	-	-	-
qwq	29.5878 ¹⁷	0.8547 ¹⁶	29.2656 ⁹	0.8521 ⁹	31.64 ¹³	0.9126 ¹³
SrDance	29.5952 ¹⁶	0.8523 ¹⁷	-	-	-	-
MLP_SR	28.6185 ¹⁸	0.8314 ¹⁸	-	-	-	-
RRDN_IITKGP	27.9708 ¹⁹	0.8085 ²⁰	-	-	29.8506 ¹⁴	0.8453 ¹⁴
congxiaofeng	26.3915 ²⁰	0.8258 ¹⁹	-	-	-	-
AiAiR	-	-	18.1903 ¹⁰	0.8245 ¹⁰	33.2633 ⁵	0.9243 ³
GDUT-SL	-	-	-	-	32.9725 ⁹	0.9204 ¹⁰

Table 2: Quantitative results of all three tracks for the AIM 2020 Real Image Super-Resolution Challenge. The superscript number indicates ranking of each metric.

5.2 AIM 2020 Challenge Results

To generate the full-size SR images for the AIM 2020 challenge, all three models from the ablation study were used for all three upscaling tracks. For $\times 4$ track, a double regression model [6] was also trained to include in the model ensemble. Each full-size LR test images were cropped to 120×120 patches and self-ensemble ($\times 8$) was applied. The cropping window was slided at 60-pixel spacing and the overlapping patches were average using weights correlated with the distance between the patch center and each pixel. With ensemble applied to all three levels, the generated full-size images were submitted to the challenge and won the first place at all three tracks. As shown in Table 2, both our PSNR and SSIM values lead the second place with a comfortable margin.

One set of representative $\times 4$ images are shown in the Fig. 6. The full-size SR output are located at the top, with selected areas zoomed in to compare with bicubic interpolation results.

6 Conclusions

In this paper, based on the models searched via GP-NAS, we have introduced a new heterogeneous model ensemble method for real image super resolution. Since network architecture greatly affects the results of SR, we first apply GP-NAS approach to search the key factors such as the number of residual network block, block size and the number of features in our network structure. Then, different models selected using GP-NAS are fused together to boost the performance of SR. Combined with patch-ensemble and self-ensemble, the proposed new scheme is validated to be highly effective, generating impressive testing results on all three tracks ($\times 2$, $\times 3$ and $\times 4$) of the AIM 2020 challenge in terms of both PSNR and SSIM.

References

- [1] Chen, L.C., Papandreou, G., Kokkinos, I., Murphy, K., Yuille, A.L.: DeepLab: Semantic image segmentation with deep convolutional nets, atrous convolution, and fully connected CRFs. *TPAMI* **40**(4), 834–848 (2017)
- [2] Chu, X., Zhang, B., Ma, H., Xu, R., Li, J., Li, Q.: Fast, accurate and lightweight super-resolution with neural architecture search. *arXiv preprint arXiv:1901.07261* (2019)
- [3] Dai, D., Wang, Y., Chen, Y., Van Gool, L.: Is image super-resolution helpful for other vision tasks? In: 2016 IEEE Winter Conference on Applications of Computer Vision (WACV). pp. 1–9. IEEE (2016)
- [4] Dong, C., Loy, C.C., He, K., Tang, X.: Learning a deep convolutional network for image super-resolution. In: European conference on computer vision. pp. 184–199. Springer (2014)
- [5] Goodfellow, I., Pouget-Abadie, J., Mirza, M., Xu, B., Warde-Farley, D., Ozair, S., Courville, A., Bengio, Y.: Generative adversarial nets. In: Advances in neural information processing systems. pp. 2672–2680 (2014)
- [6] Guo, Y., Chen, J., Wang, J., Chen, Q., Cao, J., Deng, Z., Xu, Y., Tan, M.: Closed-loop matters: Dual regression networks for single image super-resolution. In: Proceedings of the IEEE/CVF Conference on Computer Vision and Pattern Recognition. pp. 5407–5416 (2020)
- [7] Guo, Y., Luo, Y., He, Z., Huang, J., Chen, J.: Hierarchical neural architecture search for single image super-resolution. *arXiv preprint arXiv:2003.04619* (2020)
- [8] Haris, M., Shakhnarovich, G., Ukita, N.: Task-driven super resolution: Object detection in low-resolution images. *arXiv preprint arXiv:1803.11316* (2018)
- [9] Ji, X., Cao, Y., Tai, Y., Wang, C., Li, J., Huang, F.: Real-world super-resolution via kernel estimation and noise injection. In: Proceedings of the IEEE/CVF Conference on Computer Vision and Pattern Recognition Workshops. pp. 466–467 (2020)
- [10] Khattab, M.M., Zeki, A.M., Alwan, A.A., Badawy, A.S., Thota, L.S.: Multi-frame super-resolution: A survey. In: 2018 IEEE International Conference on Computational Intelligence and Computing Research (ICIC). pp. 1–8. IEEE (2018)
- [11] Kim, J., Kwon Lee, J., Mu Lee, K.: Accurate image super-resolution using very deep convolutional networks. In: Proceedings of the IEEE conference on computer vision and pattern recognition. pp. 1646–1654 (2016)
- [12] Kim, J., Kwon Lee, J., Mu Lee, K.: Deeply-recursive convolutional network for image super-resolution. In: Proceedings of the IEEE conference on computer vision and pattern recognition. pp. 1637–1645 (2016)
- [13] Krizhevsky, A., Sutskever, I., Hinton, G.E.: ImageNet classification with deep convolutional neural networks. In: Advances in neural information processing systems. pp. 1097–1105 (2012)



Figure 6: Examples of full-size test images from the AIM 2020 challenge ($\times 4$).

- [14] Ledig, C., Theis, L., Huszár, F., Caballero, J., Cunningham, A., Acosta, A., Aitken, A., Tejani, A., Totz, J., Wang, Z., et al.: Photo-realistic single image super-resolution using a generative adversarial network. In: Proceedings of the IEEE conference on computer vision and pattern recognition. pp. 4681–4690 (2017)
- [15] Li, Z., Xi, T., Deng, J., Zhang, G., Wen, S., He, R.: GP-NAS: Gaussian process based neural architecture search. In: CVPR. pp. 11933–11942 (2020)
- [16] Liang, F., Lin, C., Guo, R., Sun, M., Wu, W., Yan, J., Ouyang, W.: Computation reallocation for object detection. In: International Conference on Learning Representations (2020), <https://openreview.net/forum?id=SkxLFaNKwB>
- [17] Lim, B., Son, S., Kim, H., Nah, S., Mu Lee, K.: Enhanced deep residual networks for single image super-resolution. In: Proceedings of the IEEE conference on computer vision and pattern recognition workshops. pp. 136–144 (2017)
- [18] Liu, C., Zoph, B., Neumann, M., Shlens, J., Hua, W., Li, L.J., Fei-Fei, L., Yuille, A., Huang, J., Murphy, K.: Progressive neural architecture search. In: ECCV. pp. 19–34 (2018)
- [19] Liu, H., Simonyan, K., Vinyals, O., Fernando, C., Kavukcuoglu, K.: Hierarchical representations for efficient architecture search. arXiv preprint arXiv:1711.00436 (2017)
- [20] Liu, H., Simonyan, K., Yang, Y.: DARTS: Differentiable architecture search. arXiv preprint arXiv:1806.09055 (2018)
- [21] Ma, C., Rao, Y., Cheng, Y., Chen, C., Lu, J., Zhou, J.: Structure-preserving super resolution with gradient guidance. In: Proceedings of the IEEE/CVF Conference on Computer Vision and Pattern Recognition. pp. 7769–7778 (2020)

- [22] Ma, Y., Yu, D., Wu, T., Wang, H.: PaddlePaddle: An open-source deep learning platform from industrial practice. *Frontiers of Data and Computing* **1**(1), 105–115 (2019)
- [23] Paszke, A., Gross, S., Massa, F., Lerer, A., Bradbury, J., Chanan, G., Killeen, T., Lin, Z., Gimelshein, N., Antiga, L., Desmaison, A., Kopf, A., Yang, E., DeVito, Z., Raison, M., Tejani, A., Chilamkurthy, S., Steiner, B., Fang, L., Bai, J., Chintala, S.: Pytorch: An imperative style, high-performance deep learning library. In: Wallach, H., Larochelle, H., Beygelzimer, A., DalcheBuc, F., Fox, E., Garnett, R. (eds.) *Advances in Neural Information Processing Systems 32*, pp. 8024–8035. Curran Associates, Inc. (2019), <http://papers.neurips.cc/paper/9015-pytorch-an-imperative-style-high-performance-deep-learning-library.pdf>
- [24] Pickup, L.C., Capel, D.P., Roberts, S.J., Zisserman, A.: Bayesian methods for image super-resolution. *The Computer Journal* **52**(1), 101–113 (2009)
- [25] Song, D., Xu, C., Jia, X., Chen, Y., Xu, C., Wang, Y.: Efficient residual dense block search for image super-resolution. In: *AAAI*. pp. 12007–12014 (2020)
- [26] Sun, J., Xu, Z., Shum, H.Y.: Image super-resolution using gradient profile prior. In: *2008 IEEE Conference on Computer Vision and Pattern Recognition*. pp. 1–8. IEEE (2008)
- [27] Tai, Y.W., Liu, S., Brown, M.S., Lin, S.: Super resolution using edge prior and single image detail synthesis. In: *2010 IEEE computer society conference on computer vision and pattern recognition*. pp. 2400–2407. IEEE (2010)
- [28] Wang, Q., Tang, X., Shum, H.: Patch based blind image super resolution. In: *Tenth IEEE International Conference on Computer Vision (ICCV’05) Volume 1*. vol. 1, pp. 709–716. IEEE (2005)
- [29] Wang, X., Yu, K., Wu, S., Gu, J., Liu, Y., Dong, C., Qiao, Y., Change Loy, C.: ESRGAN: Enhanced super-resolution generative adversarial networks. In: *Proceedings of the European Conference on Computer Vision (ECCV)*. pp. 63–79 (2018)
- [30] Wei, P., Lu, H., Timofte, R., Lin, L., Zuo, W., Pan, Z., Li, B., Xi, T., Fan, Y., Zhang, G., Liu, J., Han, J., Ding, E., Xie, T., Shen, Y., Zhang, J., Jia, Y., Cheng, K., Wu, C., Lin, Y., Liu, C., Peng, Y., Zou, X., Luo, Z., Yao, Y., Xu, Z., Zamir, S.W., Arora, A., Khan, S., Hayat, M., Khan, F.S., Ahn, K.H., Kim, J.H., Choi, J.H., Lee, J.S., Zhao, T., Zhao, S., Han, Y., Kim, B.H., Baek, J., Wu, H., Xu, D., Zhou, B., Guan, W., Li, X., Ye, C., Li, H., Zhong, H., Shi, Y., Yang, Z., Yang, X., Zhong, H., Li, X., Jin, X., Wu, Y., Pang, Y., Liu, S., Liu, Z.S., Wang, L.W., Li, C.T., Cani, M.P., Siu, W.C., Zhou, Y., Umer, R.M., Micheloni, C., Cong, X., Gupta, R., Ahn, K.H., Kim, J.H., Choi, J.H., Lee, J.S., Almasri, F., Vandamme, T., Debeir, O.: AIM 2020 challenge on real image super-resolution: Methods and results. In: *Proceedings of the European Conference on Computer Vision AIM Workshop* (2020)
- [31] Yang, J., Wright, J., Huang, T., Ma, Y.: Image super-resolution as sparse representation of raw image patches. In: *2008 IEEE conference on computer vision and pattern recognition*. pp. 1–8. IEEE (2008)
- [32] Zhang, R., Isola, P., Efros, A.A., Shechtman, E., Wang, O.: The unreasonable effectiveness of deep features as a perceptual metric. In: *Proceedings of the IEEE conference on computer vision and pattern recognition*. pp. 586–595 (2018)
- [33] Zhang, Y., Li, K., Li, K., Wang, L., Zhong, B., Fu, Y.: Image super-resolution using very deep residual channel attention networks. In: *Proceedings of the European Conference on Computer Vision (ECCV)*. pp. 286–301 (2018)
- [34] Zhang, Y., Tian, Y., Kong, Y., Zhong, B., Fu, Y.: Residual dense network for image super-resolution. In: *Proceedings of the IEEE Conference on Computer Vision and Pattern Recognition*. pp. 2472–2481 (2018)
- [35] Zhou Wang, A. C. Bovik, H.R.S., Simoncelli, E.P.: Image quality assessment: from error visibility to structural similarity. *IEEE Transactions on Image Processing* **13**(4), 600–612 (2004)
- [36] Zoph, B., Le, Q.V.: Neural architecture search with reinforcement learning. *arXiv preprint arXiv:1611.01578* (2016)
- [37] Zoph, B., Vasudevan, V., Shlens, J., Le, Q.V.: Learning transferable architectures for scalable image recognition. In: *CVPR*. pp. 8697–8710 (2018)